THE JOURNAL OF PHYSICAL CHEMISTRY C

Article

Cite This: J. Phys. Chem. C 2018, 122, 1192−1196

pubs.acs.org/JPCC

Insertion and Expulsion Mechanism of an Amphiphile in a Membrane Mimetic

A. R. Ruiz-Fernández*

Department of Chemistry, Faculty of Science, University of Chile, PO Box 653, Santiago, Chile

Supporting Information

ABSTRACT: A theoretical study, validated with experimental data, on the mechanism of insertion/expulsion of an amphiphile from its aggregate is presented. Using molecular dynamics (MD), the equilibrium of tetradecyltrimethylammonium (TTA^+) between the aqueous phase and a bilayer, with TTA^+ as the main component, was simulated. In order to be inserted, the first interaction of TTA^+ with the bilayer is with the hydrophobic chain, and more importantly, before any interaction, TTA^+ has to adopt a stretched conformation along with a perpendicular orientation with respect to the aggregate surface. Otherwise, insertion fails and the amphiphile goes back into the bulk water phase. This conformation and orientation remains unmodified during the insertion and expulsion processes. Thus, this mechanism can be called the "dive in mechanism".

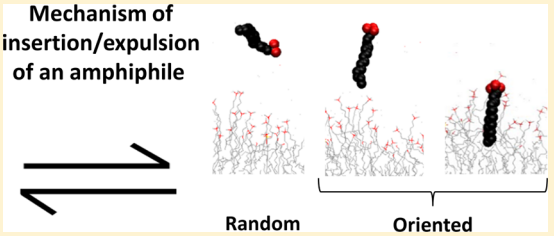

INTRODUCTION

The aggregation process of head/tail amphiphilic molecules in water has been deeply studied.[1] Nevertheless, because of experimental difficulties, the equilibrium of amphiphiles between the aqueous phase and its dissolved aggregate is much less studied. In this regard, there are several studies about unimer equilibrium exchange kinetics between micelles.[2,3] From the Halperin and Alexander theory, it is concluded that the equilibrium is mainly achieved through insertion and expulsion mechanisms of single unimers.[4,5] To obtain atomistic details on the self-assembly process of amphiphilic molecules in water, many simulation studies have been performed.[6−8] Although the insertion process of amphiphilic molecules into its aggregates has been studied,[9] the mechanism steps for insertion and expulsion of unimers with a single chain carbon from its aggregate remains unknown.

How an amphiphile, similar to the ones used in drug delivery systems[10] as templates for synthesizing nano- and mesostructured materials[11] or in membrane mimetics,[12] gets in or out from its aggregate is a basic question whose answer opens a new way for understanding the equilibrium of amphiphiles between aggregates and bulk solution, thereby giving new insights on how to manipulate the aggregation process and the stability of bilayers in general.

Nowadays exists a broad range of membrane mimetics to select according to the needs.[13] The aggregates occupied in this study are lyotropic nematic systems, developed in our laboratory, that classify as magnetically alignable bicelles, sometimes used as membrane mimetics. They are formed by aggregates of amphiphiles that adopt an discotic average geometry, called bicelles.[14] They are nematic because the order between the aggregates is only orientational (Figure 1). These systems have the advantage of being composed of bicelles, so the local morphology resembles those of biomembranes (flat bilayer). Additionally, because of their geometry, bicelles have an anisotropic diamagnetic susceptibility, which makes them align with a magnetic field, enabling the obtention of valuable information such as quadrupole splittings. They provide information regarding order and dynamics.

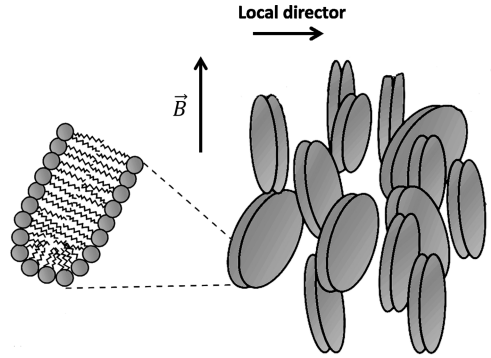

Figure 1. Representation of lyotropic nematic systems composed of magnetically alignable bicelles. $\vec{B}$ represents the magnetic field.

EXPERIMENTAL SECTION

Mesophase Preparation. The system was prepared by dissolving 0.3448 g of tetradecyltrimethylammonium chloride (TTAC), 0.1094 g of NaCl, and 0.0730 g of decanol (DeOH) in 0.995 mL of H_2O. Fully deuterated sodium dodecylsulfate (0.012 g, SDS-d_{25}) and deuterated water (5 μL, D_2O) were added per mL of water to be used as ^2H NMR probes. The system was equilibrated 48 h at 300 K before any measurement.

Received: September 29, 2017
Revised: December 18, 2017
Published: December 21, 2017

DOI: 10.1021/acs.jpcc.7b09694
J. Phys. Chem. C 2018, 122, 1192−1196

SDS-d_{25}, TTAC, and DeOH were purchased from Aldrich and used as received. Water of HPLC grade and NaCl at the highest purity available were purchased from Merck and used as received.

^{2}H NMR Spectra. ^{2}H NMR spectra were obtained in a Bruker Avance 400 NMR spectrometer, located at the Universidad de Santiago de Chile, using a broadband probe tuned to 61.425 MHz, at 300 K. The ^{2}H 90° pulse was 19 μs long, and more than 1000 transients from a spectral window of 40 kHz were accumulated in 32 kB files.

Polarized Light Microscopy (PLM). A Motic series B microscope equipped with crossed polarizers was employed to observe the liquid crystal textures. The samples were placed in a concave slide with a depth of 1 mm and were allowed to orient in a 0.84 T magnet for 15 min. Photos were taken with a 20-fold magnification, from the center of the concavity, avoiding variations in the thickness of the sample due to the curvature of the slide, at 300 K.

Computational Methods. GROMACS package 4.5.3 was used, along with the GROMOS53A6 force field.[15] For the Lennard-Jones interactions of the aliphatic chains, the force field developed by Berger et al. was used.[16] Ryckaert–Bellemans potential was used in the dihedral potential to reproduce the frequency of the trans/gauche transition of aliphatic chains.[17] These combinations of force fields have been demonstrated to successfully reproduce similar systems to the study here.[18−21]

Before the single independent simulation, the steepest descent energy minimization was applied. The initial velocities were randomly generated according with Boltzmann distribution.

The time of simulation was 1.2 μs. The integrator was the leapfrog algorithm with an integration time step size of 2 fs. van der Waals interactions were simulated using the Lennard-Jones potential (LJ), and long-range electrostatic interactions were calculated using the Particle Mesh Ewald (PME) method.[22] A cutoff of 1.0 nm was employed for the LJ and the electrostatic interactions. A linear constraint solver was used to restrain the bond lengths. Simulations were carried out in an NPT ensemble at 328 K and 1 atm, coupled to a modified Berendsen thermostat (v-rescale) and a Parrinello–Rahman barostat, with time constants of 1 and 2 ps for temperature and pressure, respectively. This temperature was necessary to reproduce the experimental data. Simulations were performed with periodic boundary conditions in all directions of space. Simple point charge (SPC) water model was employed.

RESULTS AND DISCUSSION

^{2}H NMR spectra of the studied system along with their respective PLM textures were obtained and are displayed in Figure 2. The spectral profile and the Schlieren textures observed in PLM textures confirms that the studied system corresponds to a lyotropic nematic phase.[23−27] The main component TTAC is in a concentration of 1.1809 M, largely above its CMC of 0.0047 M.[28] The signal at the center, near 0 Hz, is from D_2O, and the rest are from the deuterium of SDS-d_{25}. The separation in Hz between two signals coming from the same deuterium is the quadrupole splitting ($\Delta\nu_Q$), see Figure 2.

From the theory of magnetic resonance, $\Delta\nu_Q$ is related to the so-called "order parameter" according to eq 1. In our case, the order parameter is from the bond between carbon and deuterium (S_{CD}).

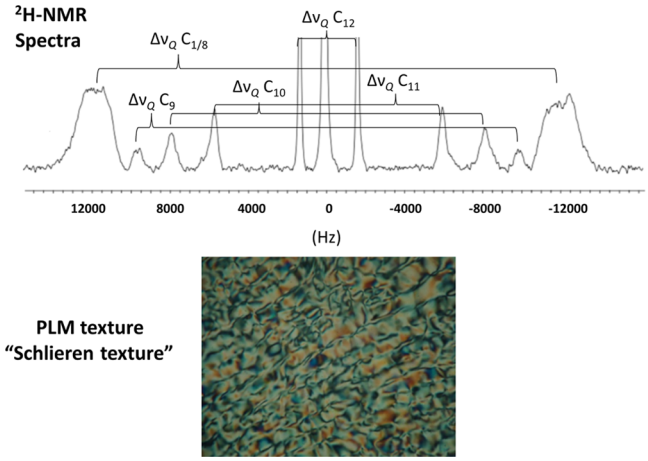

Figure 2. ^{2}H NMR spectra of SDS-d_{25} and D_2O, and the PLM texture of the studied system.

$$\Delta\nu_Q = \frac{3C\langle S_{CD}\rangle}{4} \quad (1)$$

where C is the quadrupole coupling constant (C = 170 kHz, in this case[29]), and

$$\langle S_{CD}\rangle = \frac{\langle 3\cos^2\phi - 1\rangle}{2} \quad (2)$$

where ϕ is the angle between the $C-D$ bond and the external magnetic field. This term averages to zero when the $C-D$ bond rotates isotropically or is oriented at the magic angle. In anisotropic conditions, such as that given by oriented bicelles, the $\Delta\nu_Q$ becomes different from zero. Therefore, the deuterium present in the amphiphiles that form the most oriented bicelles will give bigger $\Delta\nu_Q$ than the less oriented ones. Also two deuteriums with the same average orientation give different $\Delta\nu_Q$ if they have different amplitude of oscillation. Therefore, $\Delta\nu_Q$ depends on the orientation and dynamics of the $C-D$ bond.

To simulate the bilayer section of an aggregate forming the lyotropic nematic phase, a computational box representing the studied system was generated. This box contains the same proportion of TTA^+ and DeOH as the experimental one, disposed in a bilayer arrangement; see Figure 3, the bilayer arrangement was achieved manually with the program Visual Molecular Dynamics VMD doing first a monolayer and then duplicated and inverted it to complete the bilayer. Since the experimental proportion of dodecylsulfate anion (DS^-) only

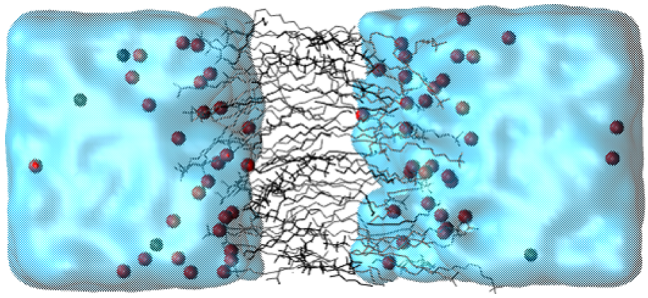

Figure 3. Representation of the simulated computational box. The cyan blob represents water, spheres in red and black represent Cl^- and Na^+ ions, respectively, and at the center are the amphiphiles TTA^+, DeOH, and DS^- as stick figures.

DOI: 10.1021/acs.jpcc.7b09694
J. Phys. Chem. C 2018, 122, 1192−1196

accomplishes two DS^- in the computational box, in order to not raise the time consumption of the simulation, the proportion of DS^- was quadrupled to enhance the sampling of $\Delta\nu_Q$ values. Na^+ and Cl^- were added to reach electroneutrality. Finally the rest of the empty space of the computational box was fulfilled with water. Water molecules situated in the hydrophobic core were removed. The computational box contained 60 TTA^+, 12 DeOH, eight DS^-, four Na^+, 60 Cl^-, and 2883 H_2O molecules. The starting dimensions of the computational box were 3.8, 3.8, and 9.1 nm, for the *x*, *y*, and *z* axis, respectively. To equilibrate the system first were simulated 500 ps in a canonical ensemble to stabilize the temperature and then 500 ps in a isothermal−isobaric ensemble to stabilize the pressure. The simulation time was 1.2 μs, and an equilibrium was rapidly achieved, registered by the plateau in the potential energy and density plots of the system (Figures 3S and 4S). A representation of the simulated computational box is displayed in Figure 3.

To validate the simulations, the experimental $\Delta\nu_Q$ (obtained from the spectrum in Figure 2) was satisfactorily reproduced, see Figure 4. To avoid the transient state, the simulated order

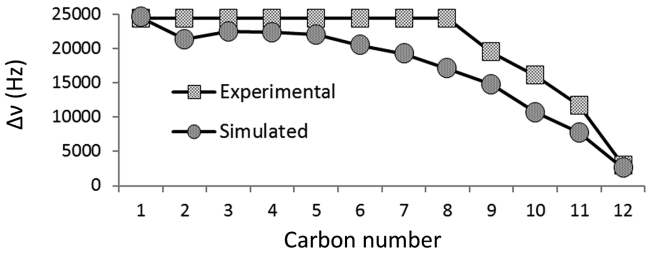

Figure 4. Simulated (circles) $\Delta\nu_Q$ and experimental (squares) $\Delta\nu_Q$ of SDS-d_{25} as a function of carbon number.

parameters were obtained as an average of all the SD^- between 10 ns and 1.2 μs. To obtain the simulated $\Delta\nu_Q$, GROMACS calculates the bond order parameter with respect to the three Cartesian axis of the box. Because bicelles orient with their principal symmetry axis perpendicular to the external magnetic field (see Figure 1), the magnetic field corresponds to *x* and *y* axes in the simulation. Thus, an average of the order parameter with respect to the *x* and *y* axes is used in eq 1 to calculate $\Delta\nu_Q$. From Figure 4 can be observed that $\Delta\nu_Q$ decreases as the carbons of SDS-d_{25} get closer to the hydrophobic core; this because the orientational order, given by the interface interaction, decreases toward the interior of the aggregate. Reproduction of the experimental $\Delta\nu_Q$ could be achieved by raising the temperature to 328 K and halving the SD^- charges. Reducing the charges is sometimes used in molecular dynamics, principally to compensate the absence of polarizability, which in conjunction with others factors overestimates electrostatic interactions.[20,30−33]

After an extensive literature search, no study regarding a simulated membrane that reproduces the equilibrium between amphiphiles in the bulk solution and amphiphiles in the aggregate was found. It is important to mention that even above the CMC some amphiphiles always remain in the bulk water solution.

Surprisingly, during the simulation, some TTA^+s spontaneously got out of the bilayer and remained in bulk solution; however, after a few nanoseconds, they got back into the aggregate. To be sure this was not an artifact, a total of 1.2 μs was simulated. During this time, an equilibrium between TTA^+s in the aggregate and in the bulk solution was achieved, see Figure 5.

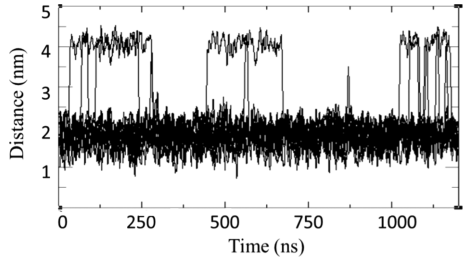

Figure 5. Distance between the center of mass of the bilayer and the center of mass of selected TTA^+s as a function of time.

During the simulation, 14 TTA^+ spontaneously leave the bilayer and 12 return to it. Figure 5 shows the distance between the center of mass of the bilayer and the center of mass of each TTA^+ that leaves the bilayer. Examining the trajectories, TTA^+s always began insertion with the carbon of the tail, adopting different orientation and conformation (Figure 1S), but one of them is by large the most probable, corresponding to an orientation with the major principal axis perpendicular to the bilayer interface and a conformation with its chain fully extended. Figure 7 shows a picture of a process representative of the insertion and expulsion of a TTA^+ from the aggregate. The LJ energy of interaction between TTA^+s and the bilayer together with the normalized projection of the major principal inertia moment in the *z* axis (I_{TTA}^z) as a function of time were plotted (Figure 7). LJ energy of 0 means that TTA^+ is in the isotropic domain (bulk), and when it begins to decrease, in the analyzing context, TTA^+ started its insertion into the membrane. If I_{TTA}^z is changing, meaning a free rotation, thus TTA^+ is in the bulk solution, and when this value is close to 1, the amphiphile is extended with a perpendicular orientation with respect to the plane of the bilayer. In Figure 7 (bottom), it can be observed that before TTA^+ gets in contact with the bilayer (LJ = 0) it adopts an orientation perpendicular to the bilayer with a fully extended conformation (I_{TTA}^z = 1) and remains that way during the entire insertion process.

Studying in detail the interaction between one TTA^+ and the bilayer while in the bulk domain, it is observed that TTA^+ has 99 independent contacts with the bilayer before insertion (LJ TTA^+/bilayer < 0), this during the 77 ns that TTA^+ is outside the bilayer (1.28 contacts/ns). The independence of each contact was established arbitrarily if it fulfills the condition of being 100 ps apart from another contact. A TTA^+ remains, in average, 68 ns in the bulk solution before its insertion; thus, one amphiphile has an average of 87 contacts (1.28 contacts/ns × 68 ns) before being inserted. Thus, the idea that an amphiphile has to be adsorbed by the interface and then immersed in the bilayer is not applicable in this case. Therefore, there must be a direct immersion into the hydrophobic core; otherwise, the insertion processes fails.

This behavior was expected mainly because the amphiphile head has the same charge as the bilayer surface, so by charge repulsion it should be the hydrophobic part of the molecule to first approach the interface. However, the requirement of having an extended chain and a perpendicular orientation, before any interaction, in order to be inserted is less expected. Even more, the carbon chain of the amphiphile in the bulk solution has a less stretched conformation (see Figure 6) and

DOI: 10.1021/acs.jpcc.7b09694
J. Phys. Chem. C 2018, 122, 1192−1196

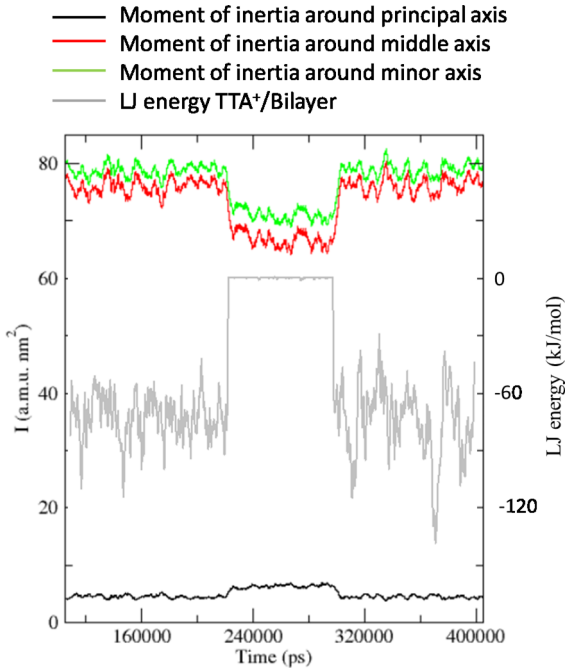

Figure 6. Moments of inertia of a representative TTA^+ around its principal, middle, and minor axes, and the LJ energy between the TTA^+ and the bilayer as a function of time.

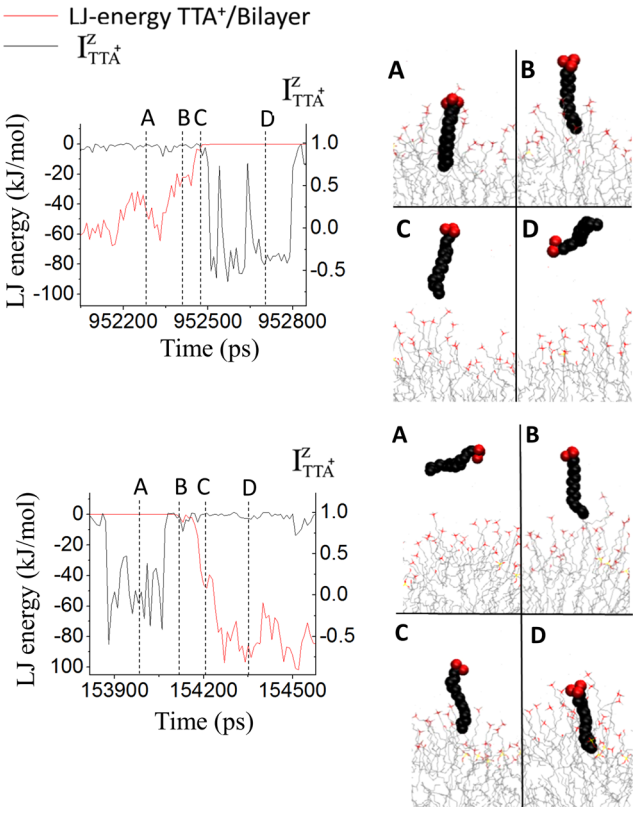

Figure 7. Mechanism of insertion (bottom) and expulsion (top) of TTA^+ from the aggregate. LJ energy between TTA^+ and the bilayer together with the normalized projection of the major principal inertia moment in the z axis ($I_{TTA}{}^z$) of TTA^+ as a function of time is also plotted.

more mobility with respect to an amphiphile inserted into the aggregate (Table 1). To represent the decrease in the stretched

Table 1. $S_D{}^2$ of the Dihedral Angles along a Representative TTA^+ Carbon Chain Inside the Bilayer and in Bulk Solution

dihedral angle	inside bilayer	bulk solution
C1−4	0.93	0.92
C2−5	0.52	0.36
C3−6	0.58	0.40
C4−7	0.54	0.43
C5−8	0.62	0.43
C6−9	0.54	0.39
C7−10	0.59	0.40
C8−11	0.56	0.38
C9−12	0.55	0.41
C10−13	0.47	0.42
C11−14	0.53	0.46

conformation when the amphiphile is expulsed from the aggregate, the moment of inertia around the principal, middle, and minor axes of a representative TTA^+ is plotted as a function of time. To represent when the TTA^+ is in the bilayer or in the bulk, the LJ energy between the TTA^+ and the bilayer is also plotted, while TTA^+ in the bilayer adopts a stretched conformation with a characteristic prolate profile observed in Figure 6. This profile is consistent with a moment of inertia around the mayor axis close to 0 and around the middle and minor axis with higher and similar values. When TTA^+ is expulsed (LJ = 0), the stretched conformation remains but with a significant decrease in its linearity, represented by a decrease of the inertia moment around the middle and minor axes and an increase of the moment of inertia around the principal axis.

The increase in TTA^+ internal mobility when it leaves the bilayer is represented by the decrease of the dihedral order parameter ($S_D{}^2$) of the dihedral angles along the TTA^+ carbon chain, see Table 1. $S_D{}^2$ was calculated for the dihedral angles formed by four consecutive carbons conforming the TTA^+ carbon chain, starting from carbon 1 (head) up to carbon 14 (tail). Each $S_D{}^2$ was obtained from the dihedral autocorrelation function,[34] from 20 ns of simulation with a time step of 2 fs.

To have a mental picture image, when Olympic divers are approaching water, they continuously change their orientation and conformation, but before entering the pool, they adopt the same conformation and orientation that TTA^+ adopts before its insertion. Thus, we can call this mechanism the "dive in mechanism".

CONCLUSIONS

The mechanism of insertion of an amphiphile in its aggregate corresponds with the expulsion one. There is a strong correlation on the conformation and orientation of the amphiphile with its displacement in an axis perpendicular to the bilayer. A stretch conformation with an orientation perpendicular to the bilayer plane facilitates this displacement and allows the insertion or expulsion of the amphiphile from the bilayer aggregate. These observations point to establish that the mechanism of insertion or expulsion of an amphiphile from its aggregate has a geometrical director. With this in mind, comprehension of the aggregation process and linked equilibriums will be improved.

ASSOCIATED CONTENT

Supporting Information

The Supporting Information is available free of charge on the ACS Publications website at DOI: 10.1021/acs.jpcc.7b09694.

DOI: 10.1021/acs.jpcc.7b09694
J. Phys. Chem. C 2018, 122, 1192−1196

Additional figures of the remaining 11 insertions and 13 expulsions, graphics of potential energy and density of the simulated system as a function of time, additional MD production data, moments of inertia not smoothed, and amphiphile self-diffusion analysis (PDF)

AUTHOR INFORMATION

Corresponding Author

*E-mail: arruiz@ug.uchile.cl. Phone: +56 951178101.

ORCID

A. R. Ruiz-Fernández: 0000-0001-6331-2261

Notes

The author declares no competing financial interest.

ACKNOWLEDGMENTS

The author is pleased to acknowledge financial support from Fondecyt-Chile (Grant No. 1150138). The author also acknowledges the assistance from the staff and facilities of the National Laboratory for High Performance Computing (NLHPC), Universidad de Chile. The author is especially grateful to Prof. Dr. Boris Weiss, from Universidad de Chile, this study could not be developed without his guide and support.

REFERENCES

(1) Sorrenti, A.; Illa, O.; Ortuno, R. Amphiphiles in aqueous solution: Well beyond a soap bubble. *Chem. Soc. Rev.* **2013**, *42*, 8200−8219.

(2) Lund, R.; Willner, L.; Stellbrink, J.; Lindner, P.; Richter, D. Logarithmic chain-exchange kinetics of diblock copolymer micelles. *Phys. Rev. Lett.* **2006**, *96*, 068302.

(3) Zinn, T.; Willner, L.; Lund, R.; Pipich, V.; Richter, D. Equilibrium exchange kinetics in n-alkyl-PEO polymeric micelles: single exponential relaxation and chain length dependence. *Soft Matter* **2012**, *8*, 623−626.

(4) Halperin, A.; Alexander, S. Polymeric micelles: their relaxation kinetics. *Macromolecules* **1989**, *22*, 2403−2412.

(5) Lu, J.; Bates, F.; Lodge, T. Chain exchange in binary copolymer micelles at equilibrium: confirmation of the independent chain hypothesis. *ACS Macro Lett.* **2013**, *2*, 451−455.

(6) Aliprandi, A.; Mauro, M.; De Cola, L. Controlling and imaging biomimetic self-assembly. *Nat. Chem.* **2016**, *8*, 10−15.

(7) Noguchi, H.; Takasu, M. Self-assembly of amphiphiles into vesicles: a Brownian dynamics simulation. *Phys. Rev. E: Stat. Phys., Plasmas, Fluids, Relat. Interdiscip. Top.* **2001**, *64*, 041913.

(8) De Vries, A. H.; Mark, A. E.; Marrink, S. J. Molecular dynamics simulation of the spontaneous formation of a small DPPC vesicle in water in atomistic detail. *J. Am. Chem. Soc.* **2004**, *126*, 4488−4489.

(9) Yu, T.; Lee, O.-S.; Schatz, G. C. Steered molecular dynamics studies of the potential of mean force for peptide amphiphile self-assembly into cylindrical nanofibers. *J. Phys. Chem. A* **2013**, *117*, 7453−7460.

(10) Malmsten, M. Soft drug delivery systems. *Soft Matter* **2006**, *2*, 760−769.

(11) Petkovich, N. D.; Stein, A. Controlling macro-and meso-structures with hierarchical porosity through combined hard and soft templating. *Chem. Soc. Rev.* **2013**, *42*, 3721−3739.

(12) Hu, Z.; Ho, J. C.; Nallani, M. Synthetic (polymer) biology (membrane): functionalization of polymer scaffolds for membrane proteins. *Curr. Opin. Biotechnol.* **2017**, *46*, 51−56.

(13) Warschawski, D. E.; Arnold, A. A.; Beaugrand, M.; Gravel, A.; Chartrand, É.; Marcotte, I. Choosing membrane mimetics for NMR structural studies of transmembrane proteins. *Biochim. Biophys. Acta, Biomembr.* **2011**, *1808*, 1957−1974.

(14) Sanders, C. R.; Prestegard, J. Magnetically orientable phospholipid bilayers containing small amounts of a bile salt analogue, CHAPSO. *Biophys. J.* **1990**, *58*, 447−460.

(15) Van Der Spoel, D.; Lindahl, E.; Hess, B.; Groenhof, G.; Mark, A. E.; Berendsen, H. J. C. GROMACS: Fast, flexible, and free. *J. Comput. Chem.* **2005**, *26*, 1701−1718.

(16) Berger, O.; Edholm, O.; Jähnig, F. Molecular dynamics simulations of a fluid bilayer of dipalmitoylphosphatidylcholine at full hydration, constant pressure, and constant temperature. *Biophys. J.* **1997**, *72*, 2002−2013.

(17) Ryckaert, J.-P.; Bellemans, A. Molecular dynamics of liquid n-butane near its boiling point. *Chem. Phys. Lett.* **1975**, *30*, 123−125.

(18) Marrink, S.-J.; Berger, O.; Tieleman, P.; Jähnig, F. Adhesion forces of lipids in a phospholipid membrane studied by molecular dynamics simulations. *Biophys. J.* **1998**, *74*, 931−943.

(19) Wang, Z.; Larson, R. G. Molecular dynamics simulations of threadlike cetyltrimethylammonium chloride micelles: effects of sodium chloride and sodium salicylate salts. *J. Phys. Chem. B* **2009**, *113*, 13697−13710.

(20) Bahamonde-Padilla, V.; Espinoza, J.; Weiss-Lopez, B.; Cascales, J. L.; Montecinos, R.; Araya-Maturana, R. Effect of lithium on the properties of a liquid crystal formed by sodium dodecylsulphate and decanol in aqueous solution. *J. Chem. Phys.* **2013**, *139*, 14703.

(21) Ruiz-Fernández, A.; López-Cascales, J.; Giner-Casares, J.; Araya-Maturana, R.; Díaz-Baños, F.; Muñoz-Gacitúa, D.; Weiss-López, B. Effect of shape and bending modulus on the properties of nematic lyotropic liquid crystals. *RSC Adv.* **2016**, *6*, 7455−7464.

(22) Darden, T.; York, D.; Pedersen, L. Particle Mesh Ewald. Am N Log(N) method for Ewalds sums in large systems. *J. Chem. Phys.* **1993**, *98*, 10089−10092.

(23) Raffard, G.; Steinbruckner, S.; Arnold, A.; Davis, J. H.; Dufourc, E. J. Temperature-composition diagram of dimyristoylphosphatidylcholine-dicaproylphosphatidylcholine bicelles self-orienting in the magnetic field. A solid state ^{2}H and ^{31}P NMR study. *Langmuir* **2000**, *16*, 7655−7662.

(24) Vermeer, L. S.; De Groot, B. L.; Réat, V.; Milon, A.; Czaplicki, J. Acyl chain order parameter profiles in phospholipid bilayers: computation from molecular dynamics simulations and comparison with ^{2}H NMR experiments. *Eur. Biophys. J.* **2007**, *36*, 919−931.

(25) Merz, K.; Roux, B.; Membranes, B. *A Molecular Perspective from Computation and Experiment*; Birkhäuser: Boston, 1996.

(26) Brown, M.; Thurmond, R.; Dodd, S.; Otten, D.; Beyer, K. Elastic deformation of membrane bilayers probed by deuterium NMR relaxation. *J. Am. Chem. Soc.* **2002**, *124*, 8471−8484.

(27) Hiltrop, K. *Lyotropic Liquid Crystals in Topics in Physical Chemistry*; Springer: New York, 1994; Vol. 3.

(28) Hoyer, H. W.; Marmo, A. The Electrophoretic Mobilities and Critical Micelle Concentrations of the Decyl-, Dodecyl-and Tetradecyltrimethylammonium Chloride Micelles and Their Mixtures. *J. Phys. Chem.* **1961**, *65*, 1807−1810.

(29) Seelig, A.; Seelig, J. The dynamic structure of fatty acyl chains in a phospholipid bilayer measured by deuterium magnetic resonance. *Biochemistry* **1974**, *13*, 4839−4845.

(30) Ahlstrom, P.; Berendsen, H. A molecular dynamics study of lecithin monolayers. *J. Phys. Chem.* **1993**, *97*, 13691−13702.

(31) López Cascales, J.; Garcia de la Torre, J.; Marrink, S.; Berendsen, H. Molecular dynamics simulation of a charged biological membrane. *J. Chem. Phys.* **1996**, *104*, 2713−2720.

(32) Poger, D.; van Gunsteren, W.; Mark, A. A New Force Field for Simulating Phosphatidylcholine Bilayers. *J. Comput. Chem.* **2010**, *31*, 1117−1125.

(33) Heinz, T.; van Gunsteren, W.; Hünenberger, P. Comparison of four methods to compute the dielectric permittivity of liquids from molecular dynamics simulations. *J. Chem. Phys.* **2001**, *115*, 1125−1136.

(34) van der Spoel, D.; Berendsen, H. Molecular dynamics simulations of Leu-enkephalin in water and DMSO. *Biophys. J.* **1997**, *72*, 2032−2041.

DOI: 10.1021/acs.jpcc.7b09694
J. Phys. Chem. C 2018, 122, 1192−1196